Amino Acids (2018) 50:141–147
https://doi.org/10.1007/s00726-017-2500-8

ORIGINAL ARTICLE

Synthetic green fluorescent protein chromophore analogues with a positive charge at the phenyl-like group

Zhao-Yi Zhang[1] · Robert Sung[2] · Kuangsen Sung[1]

Received: 19 May 2017 / Accepted: 28 September 2017 / Published online: 7 October 2017

Abstract Synthetic green fluorescent protein (GFP) chromophore analogues with a positive charge at the phenyl-like group have the highly electrophilic amidine carbon, smaller LUMO–HOMO energy gap, red-shifted electronic absorptions and fluorescent emissions, and accelerated *E-Z* thermoisomerization rates. They are water-labile and their hydrolysis results in ring-opening of the imidazolinone moiety with a half life around 25–37 h in D_2O at 25 °C.

Keywords Green fluorescent protein · Reactivity · Photophysical properties

Introduction

Green fluorescent protein (GFP) and its mutants have attracted interest as fluorescent biological labels in recent two decades (Meech 2009; Zimmer 2002). The wild-type GFP (*wt*GFP) has a globular protein of 238 amino acids that are folded into an 11-stranded β-barrel (Ormo et al. 1996; Yang et al. 1996; Suhling et al. 2002). Its chromophore, *p*-hydroxybenzylideneimidazolinone (*p*-**HBDI**), sits at the center of the β-barrel and is biosynthesized from Ser(65)-Tyr(66)-Gly(67) (Ormo et al. 1996; Yang et al. 1996; Suhling et al. 2002). The *wt*GFP has a major electronic absorption at 395 nm, which is called A band and attributed to the electronic absorption of the neutral form of the *p*-**HBDI** chromophore and a minor electronic absorption at 475 nm, which is B band and assigned to the electronic absorption of the anionic form of the *p*-**HBDI** chromophore (Heim et al. 1994; Chattoraj et al. 1996). On excitation of the A band, the A* state undergoes a rapid excited-state proton transfer (ESPT) (Tolbert et al. 2002; Han et al. 2011; Wan et al. 1993; Formosinho et al. 1993) to form the anionic I* state, which emits dominant GFP fluorescence at 508 nm with 80% quantum yield. After proton recombination, the ground-state I form quickly reforms the ground-state A form. On excitation of the B band, the B* state emits fluorescence at 503 nm. Conversion between the I and B states might involve reorganization of the surrounding protein matrix, such as isomerization of the Thr203 residue, but it occurs on a much slower timescale (Heim et al. 1994; Chattoraj et al. 1996; Brejc et al. 1997).

Due to the nature of the space and shape limitations of the protein environment, the GFP chromophore (***p*-HBDI**) inside the β-barrel can hardly decay through *Z-E* photoisomerization by 180° rotation around the I-bond (Chen et al. 2001), resulting in a high fluorescence quantum yield of 0.8 in the *wt*GFP. However, ***p*-HBDI** significantly loses fluorescence after it is stripped of the protein environment (Meech 2009; Zimmer 2002). Hence, many synthetic GFP chromophore analogues have been prepared to improve fluorescence quantum yield and/or emission properties (Yang et al. 2008; Chen et al. 2013; Lo et al. 2013; Wu et al. 2008; Huang et al. 2012; Chuang et al. 2011; Follenius-Wund et al. 2003). For our laboratory, we took advantage of low fluorescence quantum yield of ***p*-HBDI** and its analogues to develop a sensor for DNA/RNA. Because the backbone of DNA/RNA carries negative charges, we prepared synthetic GFP chromophore analogues with a

Electronic supplementary material The online version of this article (doi:10.1007/s00726-017-2500-8) contains supplementary material, which is available to authorized users.

✉ Kuangsen Sung
kssung@mail.ncku.edu.tw

[1] Department of Chemistry, National Cheng Kung University, No. 1 University Rd., Tainan, Taiwan

[2] Present Address: Faculty of Family Medicine, Northern Ontario School of Medicine, Sudbury, ON, Canada

positive charge at the phenyl-like group as a sensor for DNA/RNA. Meanwhile, to tune the properties of the GFP chromophore, we also liked to know what will happen if synthetic GFP chromophore analogues carry a positive charge at the phenyl-like group. Even though many analogues of the GFP chromophore have been prepared and studied, to our knowledge, synthetic GFP chromophore analogues with a positive charge at the phenyl-like group have not been reported yet.

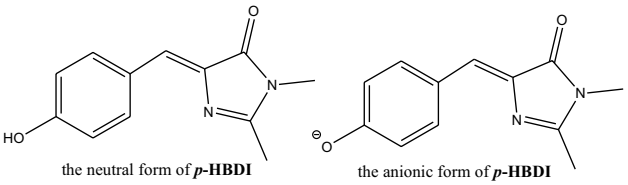

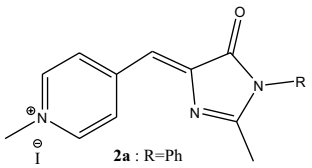

synthetic GFP chromophore analogues with a positive charge at the phenyl-like group

After we prepared synthetic GFP chromophore analogues with a positive charge at the phenyl-like group (**2a** and **2b**) and tested their DNA/RNA sensitivity in water, we found that they are labile in water. The information about how a positive charge on the phenyl-like group makes the GFP chromophore analogues labile in water and affects their various properties may be important to chemists who develop synthetic GFP chromophore analogues.

Materials and methods

Computational details

All the calculations were performed with the Gaussian09 program (Frisch et al. 2009). Geometry optimization of *p*-**HBDI**, **1a** and **2a** was carried out at the B3LYP/6-31+G* without any symmetry restriction. After the geometric optimization, analytical vibration frequencies were calculated at the same level to determine the nature of the located stationary point. The electrostatic potential maps for the electronic ground states of *p*-**HBDI**, **1a,** and **2a** were calculated at the B3LYP/6-31+G* level.

Method for measurement of fluorescence quantum yields of 1a,b and 2a,b

The fluorescence quantum yields of **1a**,**b** and **2a**,**b** were determined by the comparative method (Williams et al. 1983), and measured by comparing the wavelength-integrated intensity of the test samples to a standard. The standard used in this article is quinine sulfate in 0.1 M H_2SO_4 with the known fluorescence quantum yield of 0.577 under the excitation wavelength of 350 nm (Eastman 1967). The fluorescence quantum yields of **1a**,**b** and **2a**,**b** were calculated using

$$Q = Q_R(I/I_R)(\mathrm{OD}_R/\mathrm{OD})(n^2/n_R^2),$$

where Q is the fluorescence quantum yield, I is the integrated fluorescence intensity, n is the refractive index of the solvent, and OD is the optical density. The subscript R refers to the reference fluorophore with known fluorescence quantum yield. In this article, the reference fluorophore is quinine sulfate in 0.1 M H_2SO_4. In this method, solutions of quinine sulfate, **1a**,**b** and **2a**,**b** were illuminated with the light of the same excitation wavelength (350 nm), where quinine sulfates, **1a**,**b** and **2a**,**b,** have significant absorption. Solutions of **1a**,**b** and **2a**,**b** were prepared with optical densities in the range of 0.1–0.01 for the sake of accuracy.

General method to prepare 1a and 1b

8 mL of acetic anhydride was added isonicotinaldehyde or nicotinaldehyde (10 mmol), *N*-acetylglycine (1.17 g, 10 mmol), and sodium acetate (0.82 g, 10 mmol). The mixture was stirred in a nitrogen atmosphere at 100 °C for 75 min. After reaction, the solution was cooled by ice water. The solution was stirred until most of brown solid precipitated. After filtration, the brown solid was purified by recrystalization in aqueous EtOH.

The brown solid in 12 mL of chloroform was slowly added aniline or benzylamine (10 mmol). The mixture was stirred in a nitrogen atmosphere at room temperature for around 4.5 h until the reaction was complete. Then, the solution was concentrated by a rotary evaporator, and pyridine (7.5 mL) was added to the residue. The mixture was stirred in a nitrogen atmosphere at a reflux condition for 5 h. After reaction, the solution was cooled down and some ice was added to the solution. The solution was stirred until most of solid precipitated. The crude product was purified by column chromatography with hexane/ethyl acetate (1:1) as a mobile phase to get the product of **1a** or **1b**.

(*Z*)-2-Methyl-1-phenyl-4-(pyridin-4-ylmethylene)-1*H*-imidazol-5(4*H*)-one (**1a**). color: orange yellow; yield: 50%; ^{1}HNMR (400 MHz, $CDCl_3$) δ 2.30 (s, 3H), 7.06 (s, 1H), 7.23–7.26 (m, 2H), 7.45–7.55 (m, 3H), 8.01 (d, $J = 6.1$ Hz, 2H), 8.69(d, $J = 6.1$ Hz, 2H); ^{13}C NMR (100 MHz, $CDCl_3$) δ 16.6, 124.1, 125.2, 127.2, 129.1, 129.8, 133.0, 140.9, 141.6, 150.4, 164.4, 169.4; HRMS [FAB, $(M + H)^+$] *m*/*z* calcd for $C_{16}H_{14}N_3O$ 264.1137, found 264.1142.

(*Z*)-1-Benzyl-2-methyl-4-(pyridin-4-ylmethylene)-1*H*-imidazol-5(4*H*)-one (**1b**) color: orange yellow; yield: 70%; ^{1}HNMR (400 MHz, $CDCl_3$) δ 2.29 (s, 3H), 4.83 (s, 2H), 7.03 (s, 1H), 7.22–7.34 (m, 2H), 7.37 (m, 3H), 7.95(d, $J = 5.9$ Hz, 2H), 8.67(d, $J = 5.9$ Hz, 2H); ^{13}C NMR (100 MHz, $CDCl_3$)

δ 16.2, 44.0, 123.8, 125.2, 127.0, 128.1, 129.0, 135.6, 140.9, 141.8, 150.2, 165.1, 170.1; HRMS [FAB, $(M + H)^+$] *m/z* calcd for $C_{17}H_{16}N_3O$ 278.1290, found 278.1291.

General method to prepare 2a and 2b

1a or **1b** (2.5 mmol) in 7 mL of $CHCl_3$ was added 0.74 mL (12 mmol) of methyl iodide. The mixture was stirred in a nitrogen atmosphere at room temperature overnight until the reaction was complete. After filtration, the solid product was washed with $CHCl_3$. The product was purified by recrystallization in $CHCl_3$ to get the product of **2a** or **2b**.

(*Z*)-1-methyl-4-((2-methyl-5-oxo-1-phenyl-1*H*-imidazol-4(5*H*)-ylidene)methyl)pyridinium iodide (**2a**). color: dark brown; yield 85%;^{1}HNMR (400 MHz, D_2O) δ 2.24 (s, 3H), 4.28 (s, 3H), 7.15 (s, 1H), 7.30 (d, J = 6.5 Hz, 2H), 7.51–7.55 (m, 3H), 8.44 (d, J = 6.5 Hz, 2H), 8.68 (d, J = 6.5 Hz, 2H); ^{13}C NMR (100 MHz, DMSO) δ 17.2, 48.1, 117.6, 128.2, 128.4, 129.7, 130.1, 133.2, 145.9, 146.2, 149.4, 169.1, 170.2; HRMS [FAB, M^+] *m/z* calcd for $C_{17}H_{16}N_3O$ 278.1293, found 278.1293.

(*Z*)-1-methyl-4-((2-methyl-5-oxo-1-benzyl-1*H*-imidazol-4(5*H*)-ylidene)methyl)pyridinium iodide (**2b**). color: dark brown; yield 85%; ^{1}HNMR (400 MHz, D_2O) δ 2.31 (s, 3H), 4.27 (s, 3H), 4.83 (s, 2H), 7.12 (s, 1H), 7.23 (m, 2H), 7.32 (m, 1H), 7.35 (m, 2H), 8.39 (d, J = 6.6 Hz, 2H), 8.65 (d, J = 6.6 Hz, 2H); ^{13}C NMR (100 MHz, $CDCl_3$) δ 16.7, 44.3, 49.1, 117.0, 127.1, 128.4, 128.8, 139.2, 135.0, 145.0, 146.6, 150.0, 169.4, 170.4; HRMS [FAB, M^+] *m/z* calcd for $C_{18}H_{18}N_3O$ 292.1450, found 292.1454.

General method for hydrolysis of 2a and 2b

2a or **2b** (2 mmol) was added 5 mL of water. The mixture was stirred at room temperature until the reaction was complete. After reaction, the solution was concentrated by a rotary evaporator. The solid product was purified by recrystallization in water and acetonitrile to get the product of **3a** or **3b**.

(*Z*)-4-(2-acetamido-3-oxo-3-(phenylamino)propenyl)-1-methyl-pyridinium iodide (**3a**). yield: quantitative; ^{1}HNMR (400 MHz, D_2O) δ 2.11 (s, 3H), 4.26(s, 3H), 7.03(s, 1H), 7.24(t, J = 6.76 Hz, 1H), 7.36–7.40(m, 4H), 7.98(d, J = 6.24 Hz, 2H), 8.63(d, J = 6.2 Hz, 2H); ^{13}C NMR (100 MHz, DMSO) δ 21.7, 47.2, 120.4, 122.2, 126.0, 126.5, 128.8, 135.6, 136.1, 144.5, 150.1, 164.7, 173.2; HRMS [FAB, M^+] *m*/z calcd for $C_{17}H_{18}N_3O_2$ 296.1399, found 296.1395.

(*Z*)-4-(2-acetamido-3-oxo-3-(benzylamino)propenyl)-1-methyl-pyridinium iodide (**3b**). yield: quantitative; ^{1}HNMR (400 MHz, D_2O) δ 2.05 (s, 3H), 4.24 (s, 3H), 4.42 (s, 2H), 6.95 (s, 1H), 7.27 (m, 2H), 7.29 (m, 1H), 7.33 (m, 2H), 7.92 (d, J = 6.6 Hz, 2H), 8.61 (d, J = 6.6 Hz, 2H); ^{13}C NMR (100 MHz, D_2O) δ 22.0, 43.4, 47.6, 121.3, 126.9, 127.2, 127.5, 128.6, 128.8, 129.0, 136.1, 137.4, 144.9, 150.5, 166.4, 173.7; HRMS [FAB, M^+] *m/z* calcd for $C_{18}H_{20}N_3O_2$ 310.1558, found 310.1560.

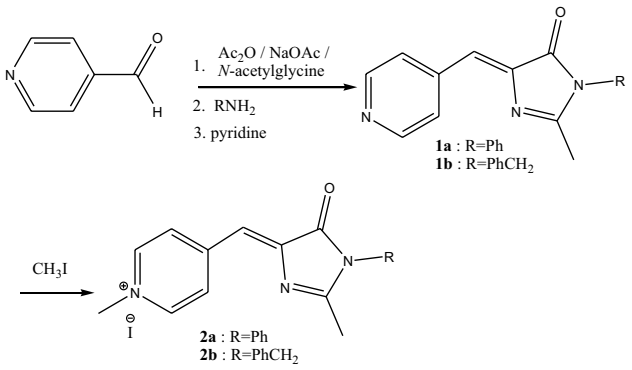

Scheme 1 Synthesis of the model compounds **2a** and **2b**

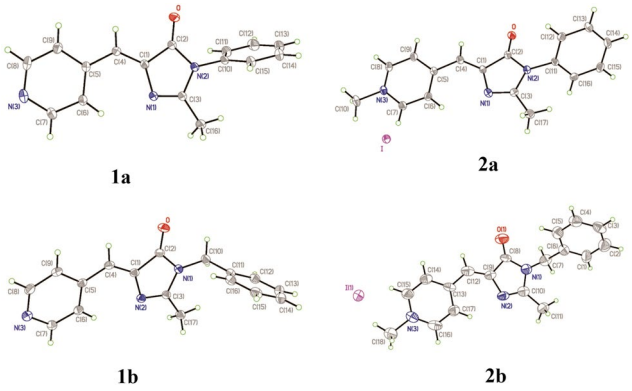

Fig. 1 Single-crystal X-ray diffraction structures of **1a**, **2a**, **1b,** and **2b** with thermal ellipsoid at the 50% probability level

Results and discussion

Synthesis and structure

Synthesis of the compounds **2a** and **2b**, which are synthetic GFP chromophore analogues with a positive charge at the phenyl-like group, is shown in Scheme 1. Reaction of isonicotinaldehyde with *N*-acetylglycine in the presence of NaOAc/Ac_2O was carried out under reflux, followed by reaction with aniline or benzylamine and cyclization in pyridine, to produce **1a** or **1b**. Methylation of **1a** and **1b** with methyl iodide generated **2a** and **2b**, respectively. According to ^{1}H and ^{13}C NMR spectra of **1a**, **1b**, **2a,** and **2b**, they all stay in single configuration. Further studies

Table 1 Electronic absorption λ_A (molar absorptivity ε), fluorescence emission λ_F (fluorescence quantum yield ϕ_f), and band gap energy ΔE of 1a, 1b, 2a, and 2b

	Solvent	$\lambda_A(\varepsilon)$	$\lambda_F(\phi_f)$	ΔE (eV)
Z-**1a**	CH_3CN	345 nm (7.5×10^3)	461 nm [$(4.5 \pm 0.3) \times 10^{-2}$]	3.15
Z-**1b**	CH_3CN	353 nm (1.3×10^4)	450 nm [$(3.0 \pm 0.2) \times 10^{-2}$]	3.11
Z-**2a**	H_2O	370 nm (7.3×10^3)	470 nm [$(1.2 \pm 0.2) \times 10^{-3}$]	2.74
Z-**2b**	CH_3CN	399 nm (1.8×10^4)	503 nm [$(9.3 \pm 0.4) \times 10^{-3}$]	2.71
	H_2O	382 nm (4.5×10^3)	498 nm [$(6.0 \pm 0.5) \times 10^{-3}$]	

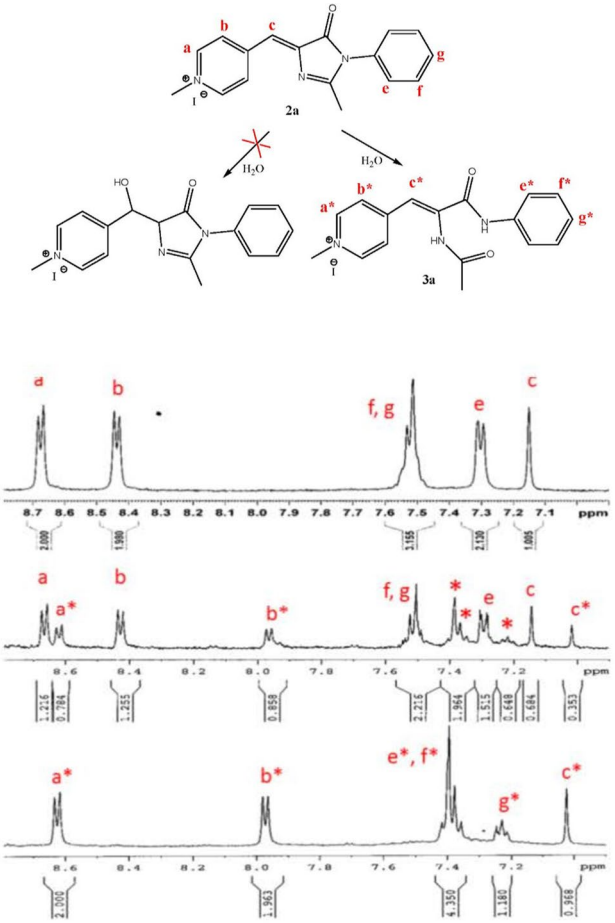

Fig. 2 ^{1}H NMR spectra of **2a** in D_2O before hydrolysis (top), 21 h after hydrolysis (middle), and at the end of hydrolysis (bottom)

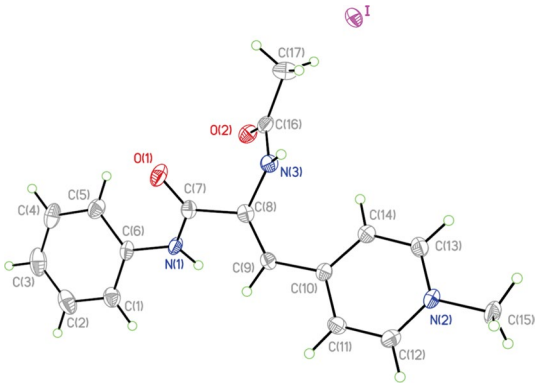

Fig. 3 Single-crystal X-ray diffraction structure of **3a** with thermal ellipsoid at the 50% probability level

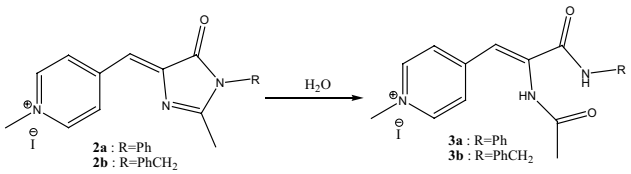

Scheme 2 Hydrolysis of the compounds **2a** and **2b**

on their configuration with single-crystal X-ray diffraction confirm that they all stay in *Z* configuration (Fig. 1).

Photophysics

As shown in Table 1 and Figs. 2 and 3, the lowest energy electronic absorptions of **1a** and **1b** in acetonitrile are located at 345 ($\varepsilon = 7.5 \times 10^3$ M^{-1} cm^{-1}) and 353 ($\varepsilon = 1.3 \times 10^4$ M^{-1} cm^{-1}), respectively. They are supposed to involve $\pi \rightarrow \pi^*$ electronic absorption. Their fluorescent emissions are located at 461 and 450 nm, respectively. Like *p*-**HBDI** (Meech 2009; Zimmer 2002), fluorescent quantum yields of **1a** and **1b** are as low as 4.5×10^{-2} and 3.0×10^{-2}. In comparison with **1a** and **1b**, the lowest energy electronic absorptions and fluorescent emissions of **2a** and **2b** in acetonitrile are all shifted to longer wavelengths, indicating that the positively charged pyridinium group in **2a** and **2b** decreases the energy gap of the chromophore between the lowest unoccupied molecular orbital (LUMO) and the highest occupied molecular orbital (HOMO).

Reactivity

The compounds **2a** and **2b** are stable in anhydrous acetonitrile and DMSO, but they are labile in alcohols and water, which are very weak nucleophiles. The whole hydrolysis processes of **2a** and **2b** were monitored by their ^{1}H NMR spectra, and only one product was formed for each of them (Fig. 2 and Scheme 2). The structure of the hydrolyzed product (**3a**) from the compound **2a** was confirmed by

Table 2 Hydrolysis rate constants [k_{D2O} (s^{-1})] of **2a,b** in D_2O at 25 °C, ^{13}C NMR chemical shifts [δ(ppm)] of the amidine carbons of **1a,b** and **2a,b**, and APT charges (Q) of the amidine carbons of **1a** and **2a**

	k_{D2O}	δ	Q
2a	$(5.22 \pm 0.89) \times 10^{-6}$	169.1	1.412
1a		164.4	0.939
2b	$(7.55 \pm 0.90) \times 10^{-6}$	169.4	
1b		165.1	

single-crystal X-ray diffraction (Fig. 3), and it proves that the amidine carbon is the only site that is attacked by very weak nucleophile of water and the rest of the structure of **2a** remains intact, resulting in ring-opening of the imidazolinone moiety. Even though the benzylidene double bond of *p*-**HBDI** analogues might be susceptible to a nucleophilic attack, according to a series of ^1H NMR spectra in Fig. 2, water nucleophile does not attack the benzylidene double bond of **2a** and **2b**.

Hydrolysis rates of the compounds **2a** and **2b** in D_2O were measured by monitoring growth of **3a** and **3b** or decay of **2a** and **2b** with ^1H NMR spectrometer at 25 °C, and their rate constants are shown in Table 2. The half lives of the hydrolysis reactions of **2a** and **2b** in D_2O were measured to be around 25–37 h.

According to the computation calculated at the B3LYP/6-31+G* level, the atomic polar tensor (APT) charge (Q) of the amidine carbon of **1a** is 0.939, and it turns to 1.412 after **2a** is produced by methylation of **1a** (Table 2). It indicates that the compound **2a** has been turned highly electrophilic at the amidine carbon in comparison with **1a**. For the ^{13}C NMR spectra of **1a**,**b** and **2a**,**b**, the resonance signals of the amidine carbons of **2a**,**b** are around 5 ppm downfield in comparison with those of **1a**,**b** (Table 2). This evidence confirms that the amidine carbons of **2a**,**b** become highly electrophilic after they are produced by methylation of **1a**,**b**.

It is interesting to know that synthetic GFP chromophore analogues with electron-withdrawing phenyl-like group, such as *p*-CF_3-phenyl and *p*-NC-phenyl groups, are stable in water (Follenius-Wund et al. 2003). Even though *p*-NO_2 group (σ_p for *p*-NO_2 = 0.78) is highly electron-withdrawing, *p*-NO_2-phenyl group (σ_p for *p*-NO_2-phenyl = 0.26) become weakly electron-withdrawing (Hansch et al. 1991). The same thing also happens to *p*-CF_3-phenyl and *p*-NC-phenyl groups. However, *p*-pyridinium group (σ_p for *p*-pyridinium = 0.58) is still highly electron-withdrawing (Hansch et al. 1991). Hence, it makes sense that **2a** and **2b** are labile in water, while synthetic GFP chromophore analogues with electron-withdrawing *p*-CF_3-phenyl and *p*-NC-phenyl groups are still stable in water.

Electronic structures

To confirm the reactivity of the positively charged *p*-**HBDI** chromophore, we calculated the electrostatic potential maps of *p*-**HBDI**, **1a,** and **2a** at B3LYP/6-31+G* level. In the electrostatic potential maps, red color represents an electron-rich area, blue color indicates an electron-deficient area, and other colors represent areas with intermediate electron density. As shown in Fig. 4, the phenol moiety of *p*-**HBDI** is electron rich and its amidine carbon is not electron deficient at all. Like *p*-**HBDI**, the electrostatic potential map of **1a** shows that its pyridine moiety is also electron-rich and its amidine carbon is not electron-deficient, either. After methylation of **1a**, not only the pyridinium moiety but also the amidine carbon become electron deficient according to the electrostatic potential map of **2a**, indicating that the amidine carbon of the positively charged *p*-**HBDI** chromophore with a positive charge at the phenyl-like group becomes highly electrophilic in comparison with **1a** and *p*-**HBDI**.

Z-E photoisomerization and ground-state *E-Z* thermoisomerization

After 20 min of irradiation with 350 nm UV light in a photo-reactor at room temperature, some of **1a**, **2a**, **1b,** and **2b** were converted to their respective *E*-isomers (Figs. 5, 6). These *E*-isomers are characterized by the downfield-shifted vinyl protons, and this is consistent with the literature (Yang et al. 2008). These *E*-isomers are less stable than their respective *Z*-isomers and will be thermally isomerized back to the respective *Z*-isomers. The *Z-E* photoisomerization and ground-state *E-Z* thermoisomerization are reproducible.

Ground-state *E-Z* thermoisomerization of *E*-**1a**,**b** and *E*-**2a**,**b** in CD_3CN or $CDCl_3$ was followed by monitoring decay of their *E*-isomers or growth of their *Z*-isomers with ^1H NMR spectroscopy (Figs. 5, 6). The *E-Z* thermoisomerization rate constants are shown in Table 3. The *E-Z* thermoisomerization rate constants of *E*-**1a**,**b** in $CDCl_3$ are larger than those in CD_3CN, indicating that the transition states of the *E-Z* thermoisomerization of *E*-**1a**,**b** are less polar than *E*-**1a**,**b**. The *E-Z* thermoisomerization rate

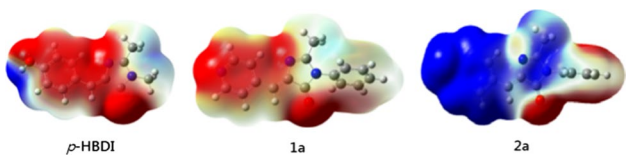

Fig. 4 Electrostatic potential maps of *p*-**HBDI**, **1a,** and **2a** at the B3LYP/6-31+G* level

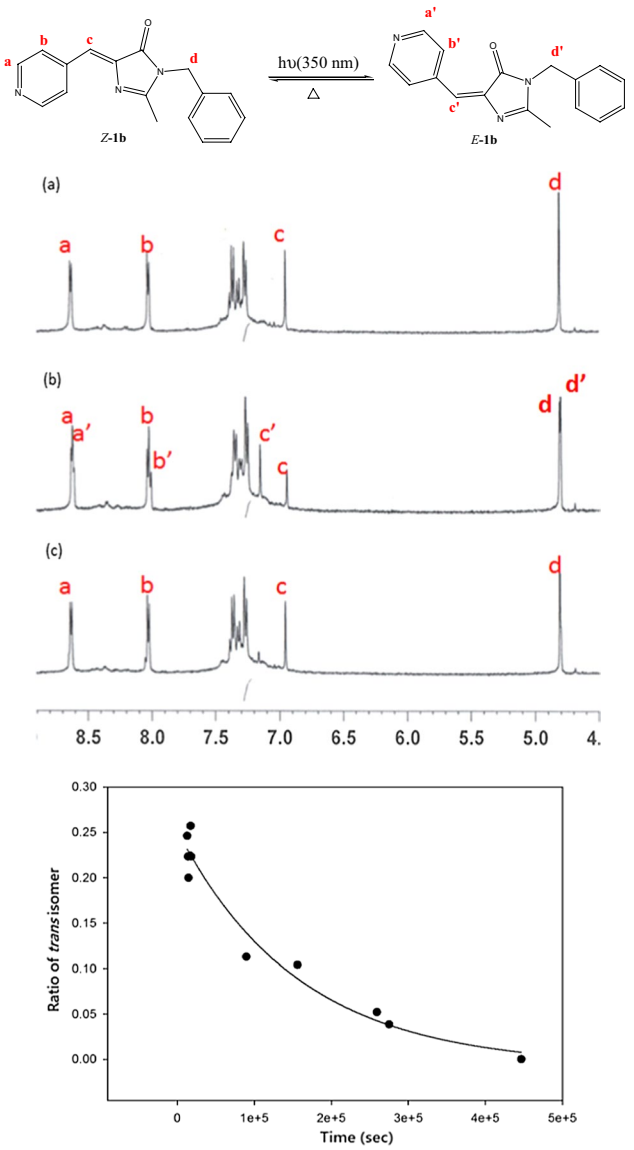

Fig. 5 ^{1}H NMR spectra of *Z*-**1b** in CD_3CN **a** before UV irradiation, **b** right after 20 min of irradiation with 350 nm UV light, and **c** 8 days after UV irradiation, and the ground-state *E*-*Z* thermoisomerization decay rate profile of *E*-**1b** in CD_3CN at 25 °C (the bottom figure)

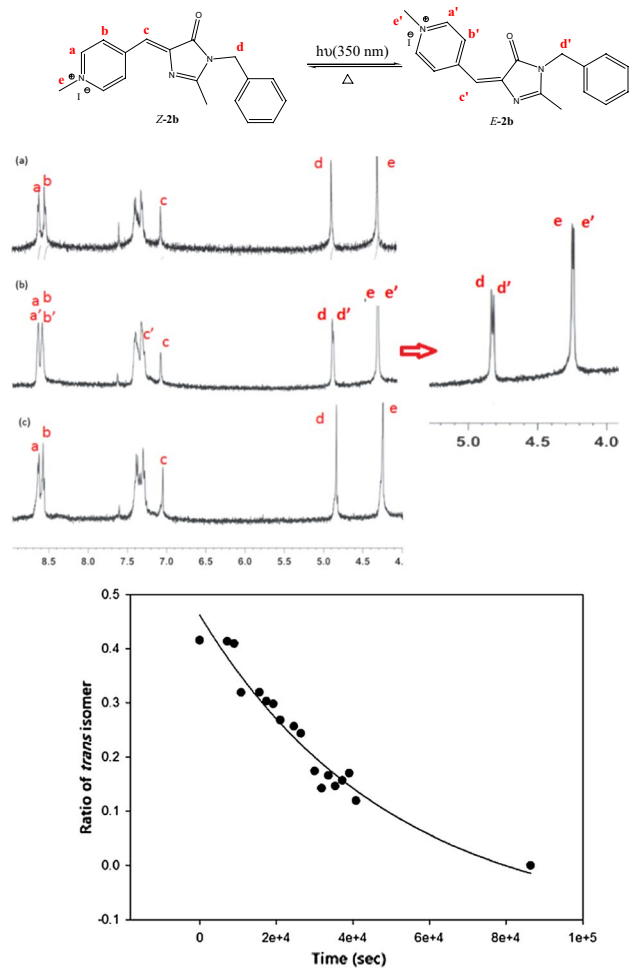

Fig. 6 ^{1}H NMR spectra of *Z*-**2b** in CD_3CN **a** before UV irradiation, **b** right after 20 min of irradiation with 350 nm UV light, and **c** 3 days after UV irradiation, and the ground-state *E*-*Z* thermoisomerization decay rate profile of *E*-**2b** in CD_3CN at 25 °C (the bottom figure)

constants of *E*-**2a**,**b**, which carry a pyridinium group, are larger than those of *E*-**1a**,**b** in CD_3CN, indicating that an electron-withdrawing group such as a pyridinium group makes the *E*-*Z* thermoisomerization rate of the *p*-**HBDI** analogues faster. This result is consistent with what Tolbert et al. found (Dong et al. 2008).

Table 3 *E*-*Z* thermoisomerization rate constants (k) of *E*-1a,b and *E*-2a,b at 25 °C

Compound	k (s^{-1}) in CD_3CN	k (s^{-1}) in $CDCl_3$
E-1a	$(1.71 \pm 0.28) \times 10^{-6}$	$(2.26 \pm 0.48) \times 10^{-5}$
E-1b	$(6.35 \pm 2.00) \times 10^{-6}$	$(8.58 \pm 0.79) \times 10^{-6}$
E-2a	$(3.74 \pm 0.55) \times 10^{-6}$	
E-2b	$(2.02 \pm 0.46) \times 10^{-5}$	

Conclusion

Like *p*-**HBDI**, its 4-pyridinyl analogues (**1a**,**b**) are stable and not easy to be hydrolyzed. After **2a**,**b** are produced by methylation of **1a**,**b**, the amidine carbons of **2a**,**b** become highly electrophilic in comparison with **1a**,**b** and labile to water and alcohols. Both the ^{13}C NMR chemical shifts and APT charges of the amidine carbons of **2a**,**b** confirm that their amidine carbons are highly electrophilic. Hydrolysis of **2a**,**b** results in ring-opening of the imidazolinone moiety. The amidine carbon of **2a**,**b** is the only site that is

attacked by very weak nucleophile of water and the rest of the structure of **2a**,**b** remains intact. The half lives of hydrolysis of **2a**,**b** are around 25–37 h.

In comparison with **1a**,**b**, the pyridinium group in **2a**,**b** accelerates the *E*-*Z* thermoisomerization rate, and also decreases the LUMO–HOMO energy gap of the chromophore, making their electronic absorptions and fluorescent emissions shifted to longer wavelengths.

Acknowledgements We thank National Science Council of Taiwan for financial support (NSC104-2119-M-006-013), and H.-L. Fu for doing some work in this research.

Compliance with ethical standards

Conflict of interest We do not have any financial conflict of interest

References

Brejc K et al (1997) Structural basis for dual excitation and photoisomerization of the *Aequorea victoria* green fluorescent protein. Proc Natl Acad Sci USA 94:2306–2311

Chattoraj M et al (1996) Ultra-fast *excited* state dynamics in green fluorescent protein: Multiple states and proton transfer. Proc Natl Acad Sci USA 93:8362–8367

Chen MC et al (2001) Photoisomerization of green fluorescent protein and the dimensions of the chromophore cavity. Chem Phys 270:157–164

Chen YH et al (2013) Synthesis, photophysical properties, and application of *o*- and *p*-amino green fluorescence protein synthetic chromophores. J Org Chem 78:301–310

Chuang WT et al (2011) Excited-state intramolecular proton transfer molecules bearing *o*-hydroxy analogues of green fluorescent protein chromophore. J Org Chem 76:8189–8202

Dong J et al (2008) Isomerization in fluorescent protein chromophores involves addition/elimination. J Am Chem Soc 130:14096–14098

Eastman JW (1967) Quantitative spectrofluorimetry—the fluorescence quantum yield of quinine sulfate. Photochem Photobiol 6:55–72

Follenius-Wund A et al (2003) Fluorescent derivatives of the GFP chromophore give a new insight into the GFP fluorescence process. Biophys J 85:1839–1850

Formosinho SJ et al (1993) Excited-state proton transfer reactions: II. Intramolecular reactions. J Photochem Photobiol A Chem 75:21–48

Frisch MJ et al. (2009) Gaussian 09, Revision E.01; Gaussian, Inc., Wallingford

Han KL et al (2011) Hydrogen bonding and transfer in the excited states. Wiley, New York

Hansch C et al (1991) A survey of Hammett substituent constants and resonance and field parameters. Chem Rev 91:165–195

Heim R et al (1994) Wavelength mutations and posttranslational autoxidation of green fluorescent protein. Proc Natl Acad Sci USA 91:12501–12504

Huang GJ et al (2012) Site-selective hydrogen-bonding-induced fluorescence quenching of highly solvatofluorochromic GFP-like chromophores. Org Lett 14:5034–5037

Lo WJ et al (2013) Twisted-based spectroscopic measure of solvent polarity: the P_T scale. J Org Chem 78:5925–5931

Meech SR (2009) Excited state reactions in fluorescent proteins. Chem Soc Rev 38:2922–2934

Ormo M et al (1996) Crystal structure of the *Aequorea victoria* green fluorescent protein. Science 273:1392–1395

Suhling K et al (2002) Imaging the environment of green fluorescent protein. Biophys J 83:3589–3595

Tolbert LM et al (2002) Excited-state proton transfer: from constrained systems to "super" photoacids to superfast proton transfer. Acc Chem Res 35:19–27

Wan P et al (1993) Utility of acid–base behaviour of excited states of organic molecules. Chem Rev 93:571–584

Williams ATR et al (1983) Relative fluorescence quantum yields using a computer controlled luminescence spectrometer. Analyst 108:1067–1071

Wu L et al (2008) Syntheses of highly fluorescent GFP-chromophore analogues. J Am Chem Soc 130:4089–4096

Yang F et al (1996) The molecular structure of green fluorescent protein. J Nat Biotechnol 14:1246–1251

Yang JS et al (2008) Photoisomerization of the green fluorescence protein chromophore and the meta- and para-amino analogues. Chem Comm. doi:10.1039/B717714C

Zimmer M (2002) Green fluorescent protein (GFP): applications, structure, and related photophysical behavior. Chem Rev 102:759–781